The Star Formation Newsletter

A community newsletter on Star and Planet Formation research

No. 335 — 20 November 2020

Editor: João Alves www.starformation.news

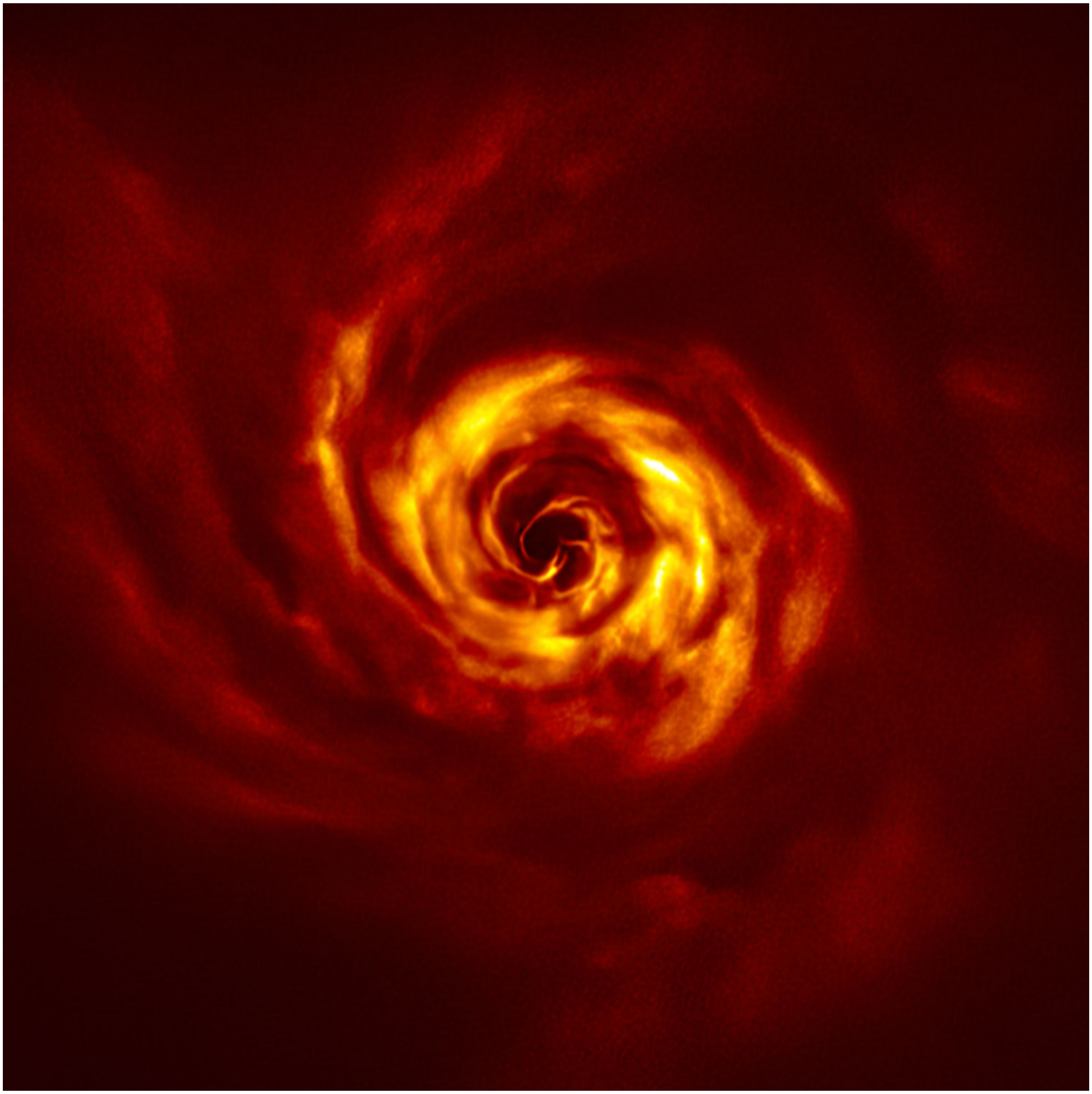

Links to sections

Cover image caption

Image of the AB Aur system in polarized light. The spiral structure can be reproduced with a planet-driven density wave model. AB Aur is a 2 $M_\odot$ young star part of the large Taurus star formation region located at about 160 pc from Earth. The star lies close to, and probably interacts with, the L1517 dark cloud. The image covers about 1000×1000 AU. Credit: ESO-VLT Sphere/Boccaletti et al.

Note from the Editor

The Star Formation Newsletter is now on the web at **www.starformation.news**. This PDF file contains the monthly Abstracts and links to the different Newsletter sections. Red text in this PDF is a url link. For the future, starting with the next SFN, please enter your abstracts, meetings, etc., on the new SFN website. Submitting an abstract on the website is as simple as entering the arXiv ID (e.g., 2006.10139) in a web form. We will extract the title, authors, and the abstract's text directly from the arXiv, so make sure not to remove the LaTeX formatting when submitting to the arXiv. If you do, your abstract will not look great either at the arXiv (which uses MathJax to convert LaTeX math symbols to the web) or the SFN. Feel free to contact me for comments and suggestions on how to improve the SFN.

Abstracts

1. A case of simultaneous star and planet formation

Felipe O. Alves, L. Ilsedore Cleeves, Josep M. Girart, Zhaohuan Zhu, Gabriel A. P. Franco, Alice Zurlo, Paola Caselli While it is widely accepted that planets are formed in protoplanetary disks, there is still much debate on when this process happens. In a few cases protoplanets have been directly imaged, but for the vast majority of systems, disk gaps and cavities – seen especially in dust continuum observations – have been the strongest evidence of recent or on-going planet formation. We present ALMA observations of a nearly edge-on ($i = 75°$) disk containing a giant gap seen in dust but not in ^{12}CO gas. Inside the gap, the molecular gas has a warm (100 K) component coinciding in position with a tentative free-free emission excess observed with the VLA. Using 1D hydrodynamic models, we find the structure of the gap is consistent with being carved by a planet with 4-70 $M_{\rm Jup}$. The coincidence of free-free emission inside the planet-carved gap points to the planet being very young and/or still accreting. In addition, the ^{12}CO observations reveal low-velocity large scale filaments aligned with the disk major axis and velocity coherent with the disk gas that we interpret as ongoing gas infall from the local ISM. This system appears to be an interesting case where both a star (from the environment and the disk) and a planet (from the disk) are growing in tandem.

2. Probing episodic accretion with chemistry: CALYPSO observations of IRAM04191+1522 Results from the CALYPSO IRAM-PdBI survey

S. Anderl, S. Maret, S. Cabrit, A. J. Maury, A. Belloche, Ph. André, A. Bacmann, C. Codella, L. Podio, F. Gueth Context. The process of mass accretion in the earliest phases of star formation is still not fully understood: Does the accretion rate smoothly decline with the age of the protostar or are there short, intermittent accretion bursts? Aims. We aim to explore whether or not the observed $C^{18}O$ and N_2H^+ emission pattern towards the VeLLO IRAM 04191+1522 can be understood in the framework of a scenario where the emission is chemically tracing a past accretion burst. Methods.We used high-angular-resolution Plateau de Bure Interferometer (PdBI) observations of $C^{18}O$ and N_2H^+ towards IRAM 04191+1522 that were obtained as part of the CALYPSO IRAM Large Program. We model these observations using a chemical code with a time-dependent physical structure coupled with a radiative transfer module, where we allow for variations in the source luminosity. Results. We find that the N_2H^+ line emission shows a central hole, while the $C^{18}O$ emission is compact. The morphology of these two lines cannot be reproduced with a constant luminosity model based on the present-day internal luminosity (0.08 L_{sun}). However, the N_2H^+ peaks are consistent with a constant-luminosity model of 12 L_{sun}. Using a model with time-dependent temperature and density profiles, we show that the observed N_2H^+ peak emission could indeed be caused by a past accretion burst. Such a burst should have occurred a couple of hundred years ago. Conclusions. We suggest that an accretion burst occurred in IRAM 04191+1522 in the recent past. If such bursts are common and sufficiently long in VeLLOs, they could lead to higher accretion onto the central object than their luminosity suggests. For IRAM 04191 in particular, our results yield an estimated final mass of 0.2 - 0.25 M_{sun} by the end of the Class 0 phase, which would make this object a low-mass star rather than a brown dwarf.

3. The role of the magnetic field in the fragmentation process: the case of G14.225-0.506

N. Añez-López, G. Busquet, P. M. Koch, J. M. Girart, H. B. Liu, F. Santos, N. L. Chapman, G. Novak, A. Palau, P. T. P. Ho, Q. Zhang B-fields are predicted to play a role in the formation of filamentary structures and their fragmentation process. We aim at investigating the role of the B-field in the process of core fragmentation toward the hub-filament systems in the IRDC G14.2, which present different fragmentation level. We performed observations of the thermal dust polarization at 350 μm using the CSO toward the hubs. We applied the polarization–intensity-gradient method to estimate the significance of the B-field over the G-force. The B-field in Hub-N shows a uniform structure along the E-W orientation, perpendicular to the major axis of the hub-filament system. The I-gradient in Hub-N displays a local minimum coinciding with the dust core MM1a detected with interferometric observations. The B-field orientation is perturbed when approaching the dust core. Hub-S shows 2 local minima, reflecting the bimodal distribution of the B-field. In Hub-N, both E and W of the hub-filament system, the I-gradient and the B-field are parallel whereas they tend to be perpendicular when penetrating the filaments and hub. The analysis of the δ- and Σ B-maps indicate that, the B-field cannot prevent the collapse, suggesting that the B-field is initially dragged by the infalling motion and aligned with it, or is channeling material toward the central ridge from both sides. Values of Σ B > 1 are found toward a N-S ridge encompassing the dust emission peak, indicating that in this region B-field dominates over G-force, or that with the current angular resolution we cannot resolve an hypothetical more complex structure. We estimated the B-field strength, the MtF ratio and the A-M number, and found differences between the 2 hubs. The different levels of fragmentation observed in these 2 hubs could arise from the differences in the B-field properties rather than from different intensity of the G-field.

4. Testing Disk Identification Methods Through Numerical Simulations of Protostellar Evolution

Yusuke Aso, Masahiro N. Machida We test whether the radii of circumstellar disks can be reliably determined in observations applying the results of a numerical simulation. Firstly, we execute a core collapse simulation which starts from a rotating magnetized spherical core, and continue the calculation until the protostellar mass reaches 0.5 Msun. Then, for each set of simulation data, we calculate the radiative transfer to generate the data cube for the synthetic observation. The spatial and velocity resolutions of the synthetic observation are 0.15 arcsec (20 au) and 0.1 km/s, respectively. We define seven different disk radii. Four radii are estimated from the synthetic observation, using the continuum image, continuum visibility, C18O channel map, and C18O position velocity (PV) diagram. The other three radii are taken from the simulation and use the disk rotation, infall motion, and density contrast around the protostar to identify the disk. Finally, we compare the disk radii estimated from the systemic observation with those from the simulation. We find that the disk radius defined using the PV diagram can reliably trace the Keplerian disk when the protostellar mass is larger than $M_* >\sim 0.2$ Msun independent of the inclination angle to the line of sight. In addition, the PV diagram provides an accurate estimate of the central stellar mass through the whole protostellar evolution. The simulation also indicates that the circumstellar disk is massive enough to be gravitationally unstable through the evolution. Such an unstable disk can show either a circular or spiral morphology on a similar timescale.

5. Formation of the Musca filament: Evidence for asymmetries in the accretion flow due to a cloud-cloud collision

L. Bonne, S. Bontemps, N. Schneider, S. D. Clarke, D. Arzoumanian, Y. Fukui, K. Tachihara, T. Csengeri, R. Guesten, A. Ohama, R. Okamoto, R. Simon, H. Yahia, H. Yamamoto Context. Dense molecular filaments are ubiquitous in the interstellar medium, yet their internal physical conditions and formation mechanism remain debated. Aims. We study the kinematics and physical conditions in the Musca filament and the Chamaeleon-Musca complex to constrain the physics of filament formation. Methods. We produced CO(2-1) isotopologue maps with the APEX telescope that cut through the Musca filament. We further study a NANTEN2 ^{12}CO(1-0) map of the Musca cloud and the HI emission of the Chamaeleon-Musca complex. Results. The Musca cloud contains multiple velocity components. Radiative transfer modelling of the CO emission indicates that the Musca filament consists of a cold ($\sim$10 K), dense ($n_{H_2} \sim 10^4$ cm^{-3}) crest, which is best described with a cylindrical geometry. Connected to the crest, a separate gas component at T$\sim$15 K and $n_{H_2} \sim 10^3$ cm^{-3} is found, the so-called strands. The filament crest has a transverse velocity gradient that is linked to the kinematics of the nearby ambient cloud. Studying the large scale kinematics, we find coherence of the asymmetric kinematics from the 50 pc HI cloud down to the Musca filament. We also report a strong [C^{18}O]/[^{13}CO] abundance drop by an order of magnitude from the filament crest to the strands over a distance < 0.2 pc in a weak far-ultraviolet (FUV) field. Conclusions. The dense Musca filament crest is a long-lived (several crossing times), dynamic structure that can form stars in the near future because of continuous mass accretion. This mass accretion appears to be triggered by a HI cloud-cloud collision, which bends the magnetic field around dense filaments. This bending of the magnetic field is then responsible for the observed asymmetric accretion scenario of the Musca filament, which is, for instance, seen as a V-shape in the position-velocity (PV) diagram.

6. ALMA chemical survey of disk-outflow sources in Taurus (ALMA-DOT). IV. Thioformaldehyde (H_2CS) in protoplanetary disks: spatial distributions and binding energies

C. Codella, L. Podio, A. Garufi, J. Perrero, P. Ugliengo, D. Fedele, C. Favre, E. Bianchi, C. Ceccarelli, S. Mercimek, F. Bacciotti, K. L. J. Rygl, L. Testi Aims: To trace the radial and vertical spatial distribution of H2CS, a key species of the S-bearing chemistry, in protoplanetary disks. To analyse the observed distributions in light of the H2CS binding energy, in order to discuss the role of thermal desorption in enriching the gas disk component. Methods: In the context of the ALMA chemical survey of Disk-Outflow sources in the Taurus star forming region (ALMA-DOT), we observed five Class I or early Class II sources with the o-H2CS(7_1,6-6_1,5) line on a 40 au scale. We estimated the binding energy (BEs) of H2CS using quantum mechanical calculations, for the first time, for an extended, periodic, crystalline ice. Results: We imaged H2CS in two rotating molecular rings in the HL Tau and IRAS04302+2247 disks. The outer radii are about 140 au (HL Tau), and 115 au (IRAS 04302+2247). The edge-on geometry of IRAS 04302+2247 reveals that H2CS emission peaks, at radii of 60-115 au, at z = $\pm$50 au from the equatorial plane. The column densities are about 10^{14} cm^{-2}. For HL Tau, we derive, for the first time, the [H2CS]/[H] abundance in a protoplanetary disk (about 10^{-14}). The BEs of H2CS computed for extended crystalline ice and amorphous ices is 4258 K and 3000-4600 K, respectively, implying a thermal evaporation where dust temperature is larger than 50-80 K. Conclusions: H2CS traces the so-called warm molecular layer, a region previously sampled using CS, and H2CO. Thioformaldehyde peaks closer to the protostar than H2CO and CS, plausibly due to the relatively high-excitation level of observed 7_1,6-6_1,5 line (60 K). The H2CS BEs implies that thermal desorption dominates in thin, au-sized, inner and/or upper disk layers, indicating that the observed H2CS emitting up to radii larger than 100 au is likely injected in the gas due to non-thermal processes.

7. Testing the star formation scaling relations in the clumps of the North American and Pelican cloud complexes

Swagat R. Das, Jessy Jose, Manash R Samal, Shaobo Zhang, Neelam Panwar The processes which regulate the star-formation within molecular clouds are still not well understood. Various star-formation scaling relations have been proposed to explain this issue by formulating a relation between star-formation rate surface density ($\Sigma_{\rm SFR}$) and the underlying gas surface density ($\Sigma_{\rm gas}$). In this work, we test various star formation scaling relations, such as Kennicutt-Schmidt relation, volumetric star-formation relation, orbital time model, crossing time model, and multi free-fall time scale model towards the North American and Pelican Nebulae complexes and in cold clumps associated with them. Measuring stellar-mass from young stellar objects and gaseous mass from CO measurements, we estimated mean $\Sigma_{\rm SFR}$, star formation rate per free-fall time, and star formation efficiency (SFE) for clumps to be 1.5 $M_\odot$ yr^{-1} kpc^{-2}, 0.009, 2.0%, respectively, while for the entire NAN complex the values are 0.6 $M_\odot$ yr^{-1} kpc^{-2}, 0.0003, and 1.6%, respectively. For clumps, we notice that the observed properties are in line with the correlation obtained between $\Sigma_{\rm SFR}$ and $\Sigma_{\rm gas}$, and between $\Sigma_{\rm SFR}$ and $\Sigma_{\rm gas}$ per free-fall time and orbital time for Galactic clouds. At the same time, we do not observe any correlation with $\Sigma_{\rm gas}$ per crossing time and multi free-fall time. Even though we see correlations in former cases, however, all models agree with each other within a factor of 0.5 dex, and discriminating between these models is not possible due to the current uncertainties in the input observables. We also test the variation of $\Sigma_{\rm SFR}$ versus the dense gas, but due to low statistics, a weak correlation is seen in our analysis.

8. Herschel Gould Belt Survey Observations of Dense Cores in the Cepheus Flare Clouds

James Di Francesco, Jared Keown, Cassandra Fallscheer, Philippe André, Bilal Ladjelate, Vera Könyves, Alexander Men'shchikov, Shaun Stephens-Whale, Quang Nguyen-Luong, Peter Martin, Sarah Sadavoy, Stefano Pezzuto, Eleonora Fiorellino, Milena Benedettini, Nicola Schneider, Sylvain Bontemps, Doris Arzoumanian, Pedro Palmeirim, Jason M. Kirk, Derek Ward-Thompson We present Herschel SPIRE and PACS maps of the Cepheus Flare clouds L1157, L1172, L1228, L1241, and L1251, observed by the Herschel Gould Belt Survey (HGBS) of nearby star-forming molecular clouds. Through modified blackbody fits to the SPIRE and PACS data, we determine typical cloud column densities of 0.5-1.0 $\times$ 10^{21} cm^{-2} and typical cloud temperatures of 14-15 K. Using the getsources identification algorithm, we extract 832 dense cores from the SPIRE and PACS data at 160-500 μm. From placement in a mass vs. size diagram, we consider 303 to be candidate prestellar cores, and 178 of these to be "robust" prestellar cores. From an independent extraction of sources at 70 μm, we consider 25 of the 832 dense cores to be protostellar. The distribution of background column densities coincident with candidate prestellar cores peaks at 2-4 $\times$ 10^{21} cm^{-2}. About half of the candidate prestellar cores in Cepheus may have formed due to the widespread fragmentation expected to occur within filaments of "transcritical" line mass. The lognormal robust prestellar core mass function (CMF) drawn from all five Cepheus clouds peaks at 0.56 $M_\odot$ and has a width of $\sim$0.5 dex, similar to that of Aquila's CMF. Indeed, the width of Cepheus' aggregate CMF is similar to the stellar system Initial Mass Function (IMF). The similarity of CMF widths in different clouds and the system IMF suggests a common, possibly turbulent origin for seeding the fluctuations that evolve into prestellar cores and stars.

9. Prestellar grain-surface origins of deuterated methanol in comet 67P/ Churyumov-Gerasimenko

Maria N. Drozdovskaya, Isaac R. H. G. Schroeder, Martin Rubin, Kathrin Altwegg, Ewine F. van Dishoeck, Beatrice M. Kulterer, Johan De Keyser, Stephen A. Fuselier, Michael Combi Deuterated methanol is one of the most robust windows astrochemists have on the individual chemical reactions forming deuterium-bearing molecules and the physicochemical history of the regions where they reside. The first-time detection of mono- and di-deuterated methanol in a cometary coma is presented for comet 67P/Churyumov-Gerasimenko using Rosetta-ROSINA data. D-methanol (CH3OD and CH2DOH combined) and D2-methanol (CH2DOD and CHD2OH combined) have an abundance of 5.5+/-0.46 and 0.00069+/-0.00014 per cent relative to normal methanol. The data span a methanol deuteration fraction (D/H ratio) in the 0.71-6.6 per cent range, accounting for statistical corrections for the location of D in the molecule and including statistical error propagation in the ROSINA measurements. It is argued that cometary CH2DOH forms from CO hydrogenation to CH3OH and subsequent H-D substitution reactions in CH3-R. CHD2OH is likely produced from deuterated formaldehyde. Meanwhile, CH3OD and CH2DOD, could form via H-D exchange reactions in OH-R in the presence of deuterated water ice. Methanol formation and deuteration is argued to occur at the same epoch as D2O formation from HDO, with formation of mono-deuterated water, hydrogen sulfide, and ammonia occurring prior to that. The cometary D-methanol/methanol ratio is demonstrated to agree most closely with that in prestellar cores and low-mass protostellar regions. The results suggest that cometary methanol stems from the innate cold (10-20 K) prestellar core that birthed our Solar System. Cometary volatiles individually reflect the evolutionary phases of star formation from cloud to core to protostar.

10. The Herschel Orion Protostar Survey: Far-Infrared Photometry and Colors of Protostars and Their Variations across Orion A and B

William J. Fischer, S. Thomas Megeath, E. Furlan, Amelia M. Stutz, Thomas Stanke, John J. Tobin, Mayra Osorio, P. Manoj, James Di Francesco, Lori E. Allen, Dan M. Watson, T. L. Wilson, Thomas Henning The degree to which the properties of protostars are affected by environment remains an open question. To investigate this, we look at the Orion A and B molecular clouds, home to most of the protostars within 500 pc. At 400 pc, Orion is close enough to distinguish individual protostars across a range of environments in terms of both the stellar and gas projected densities. As part of the Herschel Orion Protostar Survey (HOPS), we used the Photodetector Array Camera and Spectrometer (PACS) to map 108 partially overlapping square fields with edge lengths of 5 arcmin or 8 arcmin and measure the 70 micron and 160 micron flux densities of 338 protostars within them. In this paper we examine how these flux densities and their ratio depend on evolutionary state and environment within the Orion complex. We show that Class 0 protostars occupy a region of the 70 micron flux density versus 160 micron to 70 micron flux density ratio diagram that is distinct from their more evolved counterparts. We then present evidence that the Integral-Shaped Filament (ISF) and Orion B contain protostars with more massive envelopes than those in the more sparsely populated LDN 1641 region. This can be interpreted as evidence for increasing star formation rates in the ISF and Orion B or as a tendency for more massive envelopes to be inherited from denser birth environments. We also provide technical details about the map-making and photometric procedures used in the HOPS program.

11. An observational correlation between magnetic field, angular momentum and fragmentation in the envelopes of Class 0 protostars?

Maud Galametz, Anaelle Maury, Josep M. Girart, Ramprasad Rao, Qizhou Zhang, Mathilde Gaudel, Valeska Valdivia, Patrick Hennebelle, Victoria Cabedo-Soto, Eric Keto, Shih-Ping Lai To assess the potential role of magnetic fields in regulating the envelope rotation and the fragmentation of Class 0 protostars, we carried out observations of the dust polarized emission at 0.87 mm with the SMA, in the envelopes of a large sample of 20 Class 0 protostars. We estimate the mean magnetic field orientation over the central 1000 au envelope scales and compared it to that of the protostellar outflow in order to study the relation between their misalignment and the kinematics of the circumstellar gas. We discover a strong relationship between the misalignment of the magnetic field orientation with the outflow and the amount of angular momentum observed at similar scales in the protostellar envelope, revealing a potential link between the kinetic and the magnetic energy at envelope scales. The relation could be driven by favored B misalignments in more dynamical envelopes or a dependence of the envelope dynamics with the large-scale B initial configuration. Comparing the trend with the presence of fragmentation, we observe that single sources are mostly associated with conditions of low angular momentum in the inner envelope and good alignment of the magnetic field with protostellar outflows, at intermediate scales. Our results suggest that the properties of the magnetic field in protostellar envelopes bear a tight relationship with the rotating-infalling gas directly involved in the star and disk formation: we find that it may not only influence the fragmentation of protostellar cores into multiple stellar systems, but also set the conditions establishing the pristine properties of planet-forming disks.

12. Multi-directional mass-accretion and collimated outflows in W51

Ciriaco Goddi, Adam Ginsburg, Luke Maud, Qizhou Zhang, Luis Zapata We observed the W51 high-mass star-forming complex with ALMA's longest-baseline configurations, achieving an angular resolution of ∼20 milliarcseconds, corresponding to a linear resolution of ∼100 au at $D_{\rm W51} = 5.4$ kpc. The observed region contains three high-mass protostars in which the dust continuum emission at 1.3 mm is optically-thick up to a radius $\lesssim$1000 au and has brightness temperatures $\gtrsim$200 K. The high luminosity ($\gtrsim 10^4$ L$_\odot$) in the absence of free-free emission suggests the presence of massive stars ($M \gtrsim 20$ M$_\odot$) at the earliest stages of their formation. Our continuum images reveal remarkably complex and filamentary structures arising from compact cores. Molecular emission shows no clear signs of rotation nor infall on scales from 150 to 2000 au: we do not detect disks. The central sources drive young (∼100 years), fast (∼ 100 km s^{-1}), powerful ($\dot{M} > 10^{-4}$ M$_\odot$ yr^{-1}), collimated outflows. These outflows provide indirect evidence of accretion disks on scales $r \lesssim$100–500 au (depending on the object). The active outflows are connected to fossil flows that have different orientations on larger spatial scales, implying that the orientations of these small disks change over time. These results together support a variant of an accretion model for high-mass star formation in which massive protostars do not form a large, stable Keplerian disk during their early stages, but instead they accrete material from multiple massive flows with different angular momentum vectors. This scenario therefore contrasts with the simplified classic paradigm of a stable disk+jet system, which is the standard model for low-mass star formation, and provides an experimental confirmation of a multi-directional and unsteady accretion model for massive star formation.

13. STARFORGE: The effects of protostellar outflows on the IMF

Dávid Guszejnov, Michael Y. Grudić, Philip F. Hopkins, Stella S. R. Offner, Claude-André Faucher-Giguère The initial mass function (IMF) of stars is a key quantity affecting almost every field of astrophysics, yet it remains unclear what physical mechanisms determine it. We present the first runs of the STARFORGE project, using a new numerical framework to follow the formation of individual stars in giant molecular clouds (GMCs) using the GIZMO code. Our suite include runs with increasingly complex physics, starting with isothermal ideal magnetohydrodynamic (MHD) and then adding non-isothermal thermodynamics and protostellar outflows. We show that without protostellar outflows the resulting stellar masses are an order of magnitude too high, similar to the result in the base isothermal MHD run. Outflows disrupt the accretion flow around the protostar, allowing gas to fragment and additional stars to form, thereby lowering the mean stellar mass to a value similar to that observed. The effect of jets upon global cloud evolution is most pronounced for lower-mass GMCs and dense clumps, so while jets can disrupt low-mass clouds, they are unable to regulate star formation in massive GMCs, as they would turn an order unity fraction of the mass into stars before unbinding the cloud. Jets are also unable to stop the runaway accretion of massive stars, which could ultimately lead to the formation of stars with masses $> 500\,\mathrm{M}_\odot$. Although we find that the mass scale set by jets is insensitive to most cloud parameters (i.e., surface density, virial parameter), it is strongly dependent on the momentum loading of the jets (which is poorly constrained by observations) as well the the temperature of the parent cloud, which predicts slightly larger IMF variations than observed. We conclude that protostellar jets play a vital role in setting the mass scale of stars, but additional physics are necessary to reproduce the observed IMF.

14. Physical conditions of gas components in debris disks of 49 Ceti and HD 21997

Aya E. Higuchi, Ágnes Kóspál, Attila Moór, Hideko Nomura, Satoshi Yamamoto Characterization of gas component in debris disks is of fundamental importance for understanding its origin. Toward this goal, we have conducted non-LTE (local thermodynamic equilibrium) analyses of the rotational spectral lines of CO including those of rare isotopologues (^{13}CO and C^{18}O) observed toward the gaseous debris disks of 49 Ceti and HD 21997 with the Atacama Large Millimeter/submillimeter Array (ALMA) and Atacama Compact Array (ACA). The analyses have been carried out for a wide range of the H_2 density, and the observed line intensities are found to be reproduced, as far as the H_2 density is higher than 10^3 cm^{-3}. The CO column density and the gas temperature are evaluated to be (1.8-5.9)$\times 10^{17}$ cm^{-2} and 8-11 K for 49 Ceti and (2.6-15)$\times 10^{17}$ cm^{-2} and 8-12 K for HD 21997, respectively, where the H_2 collision is assumed for the rotational excitation of CO. The results do not change significantly even if electron collision is considered. Thus, CO molecules can be excited under environments of no H_2 or a small number of H_2 molecules, even where the collision with CO, C, O, and C^+ would make an important contribution for the CO excitation in addition to H_2. Meanwhile, our result does not rule out the case of abundant H_2 molecules. The low gas temperature observed in the debris disks is discussed in terms of inefficient heating by interstellar and stellar UV radiation.

15. A new prolonged decrease event in the brightness of the young stellar object V2492 Cygni

Sunay Ibryamov, Evgeni Semkov Results from the BV(RI)c photometric observations of the young stellar object V2492 Cyg collected in the period from April 2018 to September 2020 are presented. These observations are a part of our monitoring of the star that began in 2010 and continuing to date. V2492 Cyg is located in the Pelican Nebula, and its variability was explained by both accretion and extinction events. The new photometric data show that the star continues to exhibit rapid irregular variability in all bands. In the period from March 2019 to May 2020, we registered a prolonged decrease event in the light curve of V2492 Cyg.

16. The Cloud Factory II: Gravoturbulent Kinematics of Resolved Molecular Clouds in a Galactic Potential

Andres F. Izquierdo, Rowan J. Smith, Simon C. O. Glover, Ralf S. Klessen, Robin G. Tress, Mattia C. Sormani, Paul C. Clark, Ana Duarte-Cabral, Catherine Zucker We present a statistical analysis of the gravoturbulent velocity fluctuations in molecular cloud complexes extracted from our "Cloud Factory" galactic-scale ISM simulation suite. For this purpose, we produce non-LTE ^{12}CO J=1-0 synthetic observations and apply the Principal Component Analysis (PCA) reduction technique on a representative sample of cloud complexes. The velocity fluctuations are self-consistently generated by different physical mechanisms at play in our simulations, which include galactic-scale forces, gas self-gravity, and supernova feedback. The statistical analysis suggests that, even though purely gravitational effects are necessary to reproduce standard observational laws, they are not sufficient in most cases. We show that the extra injection of energy from supernova explosions plays a key role in establishing the global turbulent field and the local dynamics and morphology of molecular clouds. Additionally, we characterise structure function scaling parameters as a result of cloud environmental conditions: some of the complexes are immersed in diffuse (inter-arm) or dense (spiral-arm) environments, and others are influenced by embedded or external supernovae. In quiescent regions, we obtain time-evolving trajectories of scaling parameters driven by gravitational collapse and supersonic turbulent flows. Our findings suggests that a PCA-based statistical study is a robust method to diagnose the physical mechanisms that drive the gravoturbulent properties of molecular clouds. Also, we present a new open source module, the PCAFACTORY, which smartly performs PCA to extract velocity structure functions from simulated or real data of the ISM in a user-friendly way. Software DOI: 10.5281/zenodo.3822718

17. Evolution of the density PDF in star forming clouds: the role of gravity

Etienne Jaupart, Gilles Chabrier We derive an analytical theory of the PDF of density fluctuations in supersonic turbulence in the presence of gravity in star-forming clouds. The theory is based on a rigorous derivation of a combination of the Navier-Stokes continuity equations for the fluid motions and the Poisson equation for the gravity. It extends upon previous approaches first by including gravity, second by considering the PDF as a dynamical system, not a stationary one. We derive the transport equations of the density PDF, characterize its evolution and determine the density threshold above which gravity strongly affects and eventually dominates the dynamics of turbulence. We demonstrate the occurence of *two* power law tails in the PDF, with two characteristic exponents, corresponding to two different stages in the balance between turbulence and gravity. Another important result of this study is to provide a procedure to relate the observed *column density* PDFs to the corresponding *volume density* PDFs. This allows to infer, from the observation of column-densities, various physical parameters characterizing molecular clouds, notably the virial parameter. Furthermore, the theory offers the possibility to date the clouds in units of $t_{\rm coll}$, the time since a statistically significant fraction of the cloud started to collapse. The theoretical results and diagnostics reproduce very well numerical simulations and observations of star-forming clouds. The theory provides a sound theoretical foundation and quantitative diagnostics to analyze observations or numerical simulations of star-forming regions and to characterize the evolution of the density PDF in various regions of molecular clouds.

18. Star Formation Efficiency and Dispersal of Giant Molecular Clouds with UV Radiation Feedback: Dependence on Gravitational Boundedness and Magnetic Fields

Jeong-Gyu Kim, Eve C. Ostriker, Nina Filippova Molecular clouds are supported by turbulence and magnetic fields, but quantifying their influence on cloud lifecycle and star formation efficiency (SFE) remains an open question. We perform radiation MHD simulations of star-forming giant molecular clouds (GMCs) with UV radiation feedback, in which the propagation of UV radiation via ray-tracing is coupled to hydrogen photochemistry. We consider 10 GMC models that vary in either initial virial parameter ($1 \lesssim \alpha_v$,$0 \lesssim 5$) or dimensionless mass-to-magnetic flux ratio (0.5-8 and ∞); the initial mass 10^5 $\mathrm{M}_\odot$ and radius 20pc are fixed. Each model is run with five different initial turbulence realizations. In most models, the duration of star formation and the timescale for molecular gas removal (primarily by photoevaporation) are 4-8Myr. Both the final SFE ($\epsilon_\star$) and time-averaged SFE per freefall time (ϵff) are reduced by strong turbulence and magnetic fields. The median $\epsilon_\star$ ranges between 2.1% and 9.5%. The median ϵff ranges between 1.0% and 8.0% and anticorrelates with α_v,0, in qualitative agreement with previous analytic theory and simulations. However, the time-dependent αv(t) and ϵff,obs(t) based on instantaneous gas properties and cluster luminosity are positively correlated due to rapid evolution, making observational validation of star formation theory difficult. Our median ϵff,obs(t)$\approx$ 2% is similar to observed values. We show that the traditional virial parameter estimates the true gravitational boundedness within a factor of 2 on average, but neglect of magnetic support and velocity anisotropy can sometimes produce large departures. Magnetically subcritical clouds are unlikely to represent sites of massive star formation given their unrealistic columnar outflows, prolonged lifetime, and low escape fraction of radiation.

19. The CARMA-NRO Orion Survey: Filament Formation via Collision-Induced Magnetic Reconnection – The Stick in Orion A

Shuo Kong, Volker Ossenkopf-Okada, Héctor G. Arce, John Bally, Álvaro Sánchez-Monge, Peregrine McGehee, Sümeyye Suri, Ralf S. Klessen, John M. Carpenter, Dariusz C. Lis, Fumitaka Nakamura, Peter Schilke, Rowan J. Smith, Steve Mairs, Alyssa Goodman, María José Maureira A unique filament is identified in the *Herschel* maps of the Orion A giant molecular cloud. The filament, which, we name the Stick, is ruler-straight and at an early evolutionary stage. Transverse position-velocity diagrams show two velocity components closing in on the Stick. The filament shows consecutive rings/forks in $C^{18}O$(1-0) channel maps, which is reminiscent of structures generated by magnetic reconnection. We propose that the Stick formed via collision-induced magnetic reconnection (CMR). We use the magnetohydrodynamics (MHD) code Athena++ to simulate the collision between two diffuse molecular clumps, each carrying an anti-parallel magnetic field. The clump collision produces a narrow, straight, dense filament with a factor of >200 increase in density. The production of the dense gas is seven times faster than free-fall collapse. The dense filament shows ring/fork-like structures in radiative transfer maps. Cores in the filament are confined by surface magnetic pressure. CMR can be an important dense-gas-producing mechanism in the Galaxy and beyond.

20. Probing the Cold Deep Depths of the California Molecular Cloud: The Icy Relationship between CO and Dust

John Arban Lewis, Charles Lada, John Bieging, Anoush Kazarians, João Alves, Marco Lombardi We study the relationship between molecular gas and dust in the California Molecular Cloud over an unprecedented dynamic range of cloud depth (Av = 3 - 60 magnitudes). We compare deep Herschel-based measurements of dust extinction with observations of the 12CO, 13CO, and C18O J=2-1 lines on sub-parsec scales across the cloud. We directly measure the ratio of CO integrated intensity to dust extinction to derive the CO X-factor at over 1e5 independent locations in the cloud. Confirming an earlier study, we find that no single 12CO X-factor can characterize the molecular gas in the cold (Tdust<20K) regions of the cloud that account for most of its mass. We are able to derive a single-valued X-factor for all three CO isotopologues in the warm (Tdust>25 K) material that is spatially coincident with an HII region surrounding the star LKHa101. We derive LTE CO column densities for 13CO and C18O since we find both lines are relatively optically thin. In the warm cloud material CO is completely in the gas phase and we are able to recover the total 13CO and C18O abundances. Using CO abundances and deep Herschel observations, we measure lower bounds to the freeze-out of CO onto dust across the whole cloud finding some regions having CO depleted by a factor of >20. We construct the first maps of depletion that span the extent of a giant molecular cloud. Using these maps we identify 75 depletion-defined cores and discuss their physical nature.

21. Characterization of very wide companion candidates to young stars with planets and disks

F. Z. Majidi, S. Desidera, J. M. Alcalá, A. Frasca, V. D'Orazi, M. Bonnefoy, R. Claudi, R. Gratton, D. Mesa Discovering wide companions of stellar systems allows us to constrain the dynamical environment and age of the latter. We studied four probable wide companions of four different stellar systems. The central stars are V4046 Sgr, HIP 74865, HIP 65426, and HIP 73145, and their probable wide companions are 2MASS J18152222-3249329, 2MASS J15174874-3028484, 2MASS J13242119-5129503, and 2MASS J14571503-3543505 respectively. V4046 Sgr is a member of β-Pictoris Moving Group while the rest of the stellar systems are acknowledged as members of the Scorpius-Centaurus association. The selected stellar systems are particularly interesting because all of them are already known to possess a low-mass companion and/or a spatially resolved disk. Identifying wider companions of these stars can improve their eligibility as benchmarks for understanding the formation channels of various triple systems, and can help us to determine the orbits of their possibly undiscovered inner, wider companions in case of higher multiplicity. We find that 2MASS J15174874-3028484 (0.11 $M_\odot$, 7.4±0.5 Myr), an already recognized pre-main sequence (PMS) member of Scorpius-Centaurus association, is a highly probable wide companion of HIP 74865. 2MASS J13242119-5129503 (0.04 $M_\odot$, 16±2.2 Myr) is ruled out as a plausible wide companion of HIP 65426, but confirmed to be a new sub-stellar member of the Scorpius-Centaurus association. 2MASS J14571503-3543505 (0.02 $M_\odot$, 17.75±4.15 Myr) is a probable sub-stellar member of the same association, but we cannot confirm whether or not it is gravitationally bound to HIP 73145. 2MASS J18152222-3249329 (0.3 $M_\odot$, older than 150 Myr) is determined to be a mildly active main sequence (MS) star, much older than members of β-Pictoris Moving Group, and unbound to V4046 Sgr despite their similar kinematic features.

22. Untangling Magnetic Complexity in Protoplanetary Disks with the Zeeman Effect

Renato Mazzei, L. Ilsedore Cleeves, Zhi-Yun Li With the recent advent of circular polarization capabilities at the Atacama Large Millimeter/submillimeter Array (ALMA), Zeeman effect measurements of spectral lines are now possible as a means to directly probe line-of-sight magnetic fields in protoplanetary disks (PPDs). We present a modeling study that aims to guide physical interpretation of these anticipated observations. Using a fiducial density structure based on a typical ringed disk, we simulate line emission for the hyperfine components of the CN $J = 1 - 0$ transition with the POLARIS radiative transfer code. Since the expected magnetic field and typical CN distribution in PPDs remain largely unconstrained, we produce models with several different configurations. Corresponding integrated Stokes I and V profiles and 0.4 km/s resolution, 1" beam convolved channel maps are presented. We demonstrate that the emission signatures from toroidally dominated magnetic fields are distinguishable from vertically dominated magnetic field based on channel map morphology. Due to line-of-sight and beam cancellation effects, disks with toroidal $\boldsymbol{B}$-field configurations result in significantly diminished Stokes V emission. Complex magnetic fields therefore render the traditionally used method for inferring line-of-sight magnetic field strengths (i.e., fitting the derivative of the Stokes I to the Stokes V profile) ambiguous, since a given intrinsic field strength can yield a variety of Stokes V amplitudes depending on the magnetic field geometry. In addition, gas gaps can create structure in the integrated Stokes V profile that might mimic magnetic substructure. This method should therefore be applied with caution in PPD environments, and can only confidently be used as a measure of magnetic field strength if the disk's magnetic field configuration is well understood.

23. On the compressive nature of turbulence driven by ionising feedback in the pillars of the Carina Nebula

Shyam H. Menon, Christoph Federrath, Pamela Klaassen, Rolf Kuiper, Megan Reiter The ionizing radiation of massive stars sculpts the surrounding neutral gas into pillar-like structures. Direct signatures of star formation through outflows and jets are observed in these structures, typically at their tips. Recent numerical simulations have suggested that this star formation could potentially be triggered by photoionising radiation, driving compressive modes of turbulence in the pillars. In this study we use recent high-resolution ALMA observations of ^{12}CO, ^{13}CO, and C^{18}O, $J = 2-1$ emission to test this hypothesis for pillars in the Carina Nebula. We analyse column density and intensity-weighted velocity maps, and subtract any large-scale bulk motions in the plane of the sky to isolate the turbulent motions. We then reconstruct the dominant turbulence driving mode in the pillars, by computing the turbulence driving parameter b, characterised by the relation $\sigma_{\rho/\rho_0} = b\mathcal{M}$ between the standard deviation of the density contrast σ_{ρ/ρ_0} (with gas density ρ and its average ρ_0) and the turbulent Mach number $\mathcal{M}$. We find values of $b \sim 0.7$–1.0 for most of the pillars, suggesting that predominantly compressive modes of turbulence are driven in the pillars by the ionising radiation from nearby massive stars. We find that this range of b values can produce star formation rates in the pillars that are a factor ~ 3 greater than with $b \sim 0.5$, a typical average value of b for spiral-arm molecular clouds. Our results provide further evidence for the potential triggering of star formation in pillars through compressive turbulent motions.

24. Dense cores in the Seahorse infrared dark cloud: physical properties from modified blackbody fits to the far-infrared-submillimetre spectral energy distributions

Oskari Miettinen We used data from WISE, IRAS, and Herschel in conjuction with our previous observations with SABOCA and LABOCA, and constructed the far-IR to submillimetre spectral energy distributions (SEDs) of dense cores in the filamentary Seahorse infrared dark cloud (IRDC) G304.74+01.32. For the 12 analysed cores, which include two IR dark cores (no WISE counterpart), nine IR bright cores, and one HII region, the mean dust temperature of the cold (warm) component, the mass, luminosity, H_2 number density, and surface density were derived to be 13.3 ± 1.4 K (47.0 ± 5.0 K), 113 ± 29 M$_\odot$, 192 ± 94 L$_\odot$, $(4.3 \pm 1.2) \times 10^5$ cm^{-3}, and 0.77 ± 0.19 g cm^{-3}, respectively. The HII region IRAS 13039-6108a was found to be the most luminous source in our sample ($(1.1 \pm 0.4) \times 10^3$ L$_\odot$). All the cores were found to be gravitationally bound (i.e. the virial parameter $\alpha_{\rm vir} < 2$). Seven out of 12 of the analysed cores (58to lie above the mass-radius thresholds of high-mass star formation proposed in the literature. The surface densities of $\Sigma > 0.4$ g cm^{-3} derived for these seven cores also exceed the corresponding threshold for high-mass star formation. Five of the analysed cores (42two components in the SABOCA 350 μm image. In addition to the HII region source IRAS 13039-6108a, some of the other cores in Seahorse also appear to be capable of giving birth to high-mass stars. The dense core population in the Seahorse IRDC has comparable average properties to the cores in the well-studied Snake IRDC G11.11-0.12. The Seahorse core fragmentation mechanisms appear to be heterogenous, including cases of both thermal and non-thermal Jeans instability. High-resolution follow-up studies are required to address the fragmented cores' genuine potential of forming high-mass stars.

25. New Herbig-Haro objects and outflows in Mon R1 association

T. A. Movsessian, T. Yu. Magakian, S. N. Dodonov We present results of the narrow-band Halpha and [SII] imaging survey of Mon R1 association, performed with the 1 m Schmidt telescope of the Byurakan Observatory. Our observations covered one degree field near the center of the association. As a result of this study twenty new Herbig-Haro knots were discovered, some of which form collimated outflows. Among the most extended ones are HH 1203 and HH 1196, which have a length near one parsec or even more. In the course of search for the probable sources of HH objects several new nebulous stars were found. A list of all nebulous stellar objects in the Mon R1 area under study is presented, with the detailed description of most interesting objects. The near infrared data from the GLIMPSE360 and WISE surveys allowed to find several more objects, related to Mon R1, some of them with optical counterparts, as well as to outline at least three probable H_2 collimated flows from the deeply embedded pre-main-sequence objects. The probable members of Mon R1 were selected by their distances, their bolometric luminosities and extinctions were estimated. Among the outflow sources three embedded objects with luminosities greater than 10 L(sun) were found. The mean distance to Mon R1 complex is estimated as 715 pc.

26. ALMA chemical survey of disk-outflow sources in Taurus (ALMA-DOT) III: The interplay between gas and dust in the protoplanetary disk of DG Tau

L. Podio, A. Garufi, C. Codella, D. Fedele, K. Rygl, C. Favre, F. Bacciotti, E. Bianchi, C. Ceccarelli, S. Mercimek, R. Teague, L. Testi Planets form in protoplanetary disks and inherit their chemical composition. It is therefore crucial to understand the disks molecular content. We aim to characterize the distribution and abundance of molecules in the disk of DG Tau. In the context of the ALMA chemical survey of Disk-Outflow sources in Taurus (ALMA-DOT) we analyse ALMA observations of the disk of DG Tau in H2CO 3(1,2)-2(1,1), CS 5-4, and CN 2-1 at 0.15", i.e. 18 au at 121 pc. H2CO and CS originate from a disk ring at the edge of the 1.3mm dust continuum, with CS probing an outer disk region with respect to H2CO (peaking at 70 and 60 au, respectively). CN originates from an outermost disk/envelope region peaking at 80 au. H2CO is dominated by disk emission, while CS probes also two streams of material possibly accreting onto the disk with a peak of emission where the stream connects to the disk. The ring- and disk-height- averaged column densities are 2.4-8.6e13 cm-2 (H2CO), 1.7-2.5e13 cm-2 (CS), and 1.9-4.7e13 cm-2 (CN). Unsharp masking reveals a ring of enhanced dust emission at 40 au, i.e. just outside the CO snowline (30 au). CS and H2CO emissions are co-spatial suggesting that they are chemically linked. The observed rings of molecular emission at the edge of the 1.3mm continuum may be due to dust opacity effects and/or continnum over-subtraction in the inner disk; as well as to increased UV penetration and/or temperature inversion at the edge of the mm-dust which would cause an enhanced gas-phase formation and desorption of these molecules. Moreover, H2CO and CS originate from outside the ring of enhanced dust emission, which also coincides with a change of the linear polarization at 0.87mm. This suggests that outside the CO snowline there could be a change of the dust properties which would reflect in the increase of the intensity (and change of polarization) of continuum, and of molecular emission.

27. The VLA/ALMA Nascent Disk and Multiplicity (VANDAM) Survey of Orion Protostars IV. Unveiling the Embedded Intermediate-Mass Protostar and Disk within OMC2-FIR3/HOPS-370

John J. Tobin, Patrick Sheehan, Nickalas Reynolds, S. Thomas Megeath, Mayra Osorio, Guillem Anglada, Ana Karla Diaz-Rodriguez, Elise Furlan, Kaitlin Kratter, Stella Offner, Leslie Looney, Mihkel Kama, Zhi-Yun Li, Merel van't Hoff, Sarah Sadavoy, Nicole Karnath We present ALMA (0.87 mm and 1.3 mm) and VLA (9 mm) observations toward the candidate intermediate-mass protostar OMC2-FIR3 (HOPS-370; L_{bol} 314 $L_\odot$) at $\sim$0.1" (40 au) resolution for the continuum emission and 0.25" (100 au) resolution of nine molecular lines. The dust continuum observed with ALMA at 0.87 mm and 1.3 mm resolve a near edge-on disk toward HOPS-370 with an apparent radius of 100 au. The VLA observations detect both the disk in dust continuum and free-free emission extended along the jet direction. The ALMA observations of molecular lines (H_2CO, SO, CH_3OH, ^{13}CO, $C^{18}O$, NS, and $H^{13}CN$) reveal rotation of the apparent disk surrounding HOPS-370 orthogonal to the jet/outflow direction. We fit radiative transfer models to both the dust continuum structure of the disk and molecular line kinematics of the inner envelope and disk for the H_2CO, CH_3OH, NS, and SO lines. The central protostar mass is determined to be $\sim$2.5 $M_\odot$ with a disk radius of $\sim$94 au, when fit using combinations of the H_2CO, CH_3OH, NS, and SO lines, consistent with an intermediate-mass protostar. Modeling of the dust continuum and spectral energy distribution (SED) yields a disk mass of 0.035 $M_\odot$ (inferred dust+gas) and a dust disk radius of 62 au, thus the dust disk may have a smaller radius than the gas disk, similar to Class II disks. In order to explain the observed luminosity with the measured protostar mass, HOPS-370 must be accreting at a rate between 1.7 and 3.2×10^{-5} $M_\odot$ yr^{-1}.

28. Statistics of wide pre-main sequence binaries in the Orion OB1 association

Andrei Tokovinin, Monika Petr-Gotzens, Cesar Briceno Statistics of low-mass pre-main sequence binaries in the Orion OB1 association with separations ranging from 0.6" to 20" (220 to 7400 au at 370 pc) are studied using images from the VISTA Orion mini-survey and astrometry from Gaia. The input sample based on the CVSO catalog contains 1137 stars of K and M spectral types (masses between 0.3 and 0.9 Msun), 1021 of which are considered to be association members. There are 135 physical binary companions to these stars with mass ratios above 0.13. The average companion fraction is 0.09+-0.01 over 1.2 decades in separation, slightly less than, but still consistent with, the field. We found a difference between the Ori OB1a and OB1b groups, the latter being richer in binaries by a factor 1.6+-0.3. No overall dependence of the wide-binary frequency on the observed underlying stellar density is found, although in the Ori OB1a off-cloud population these binaries seem to avoid dense clusters. The multiplicity rates in Ori OB1 and in sparse regions like Taurus differ significantly, hinting that binaries in the field may originate from a mixture of diverse populations.

29. On the diversity of asymmetries in gapped protoplanetary disks

Nienke van der Marel, Til Birnstiel, Antonio Garufi, Enrico Ragusa, Valentin Christiaens, Daniel Price, Steph Sallum, Dhruv Muley, Logan Francis, Ruobing Dong Protoplanetary disks with large inner dust cavities are thought to host massive planetary or substellar companions. These disks show asymmetries and rings in the millimeter continuum, caused by dust trapping in pressure bumps, and potentially vortices or horseshoes. The origin of the asymmetries and their diversity remains unclear. We present a comprehensive study of 16 disks for which the gas surface density profile has been constrained by CO isotopologue data. We compare the azimuthal extents of the dust continuum profiles with the local gas surface density in each disk, and find that the asymmetries correspond to higher Stokes numbers or low gas surface density. We discuss which asymmetric structures can be explained by a horseshoe, a vortex or spiral density waves. Second, we reassess the gas gap radii from the ^{13}CO maps, which are about a factor 2 smaller than the dust ring radii, suggesting that companions in these disks are in the brown dwarf mass regime ($\sim 15-50 M_{\rm Jup}$) or in the Super-Jovian mass regime ($\sim 3-15 M_{\rm Jup}$) on eccentric orbits. This is consistent with the estimates from contrast curves on companion mass limits. These curves rule out (sub)stellar companions ($q >$0.05) for the majority of the sample at the gap location, but it remains possible at even smaller radii. Third, we find that spiral arms in scattered light images are primarily detected around high luminosity stars with disks with wide gaps, which can be understood by the dependence of the spiral arm pitch angle on disk temperature and companion mass.

30. Striations, integrals, hourglasses and collapse – thermal instability driven magnetic simulations of molecular clouds

C. J. Wareing, J. M. Pittard, S. A. E. G. Falle The MHD version of the adaptive mesh refinement (AMR) code, MG, has been employed to study the interaction of thermal instability, magnetic fields and gravity through 3D simulations of the formation of collapsing cold clumps on the scale of a few parsecs, inside a larger molecular cloud. The diffuse atomic initial condition consists of a stationary, thermally unstable, spherical cloud in pressure equilibrium with lower density surroundings and threaded by a uniform magnetic field. This cloud was seeded with 10% density perturbations at the finest initial grid level around n=1.1 cm^{-3} and evolved with self-gravity included from the outset. Several cloud diameters were considered (100 pc, 200 pc and 400 pc) equating to several cloud masses (17,000 Msun, 136,000 Msun and 1.1x10^6 Msun). Low-density magnetic-field-aligned striations were observed as the clouds collapse along the field lines into disc-like structures. The induced flow along field lines leads to oscillations of the sheet about the gravitational minimum and an integral-shaped appearance. When magnetically supercritical, the clouds then collapse and generate hourglass magnetic field configurations with strongly intensified magnetic fields, reproducing observational behaviour. Resimulation of a region of the highest mass cloud at higher resolution forms gravitationally-bound collapsing clumps within the sheet that contain clump-frame supersonic (M$\sim$5) and super-Alfvenic (M$_A\sim$4) velocities. Observationally realistic density and velocity power spectra of the cloud and densest clump are obtained. Future work will use these realistic initial conditions to study individual star and cluster feedback.

31. The JCMT BISTRO survey: alignment between outflows and magnetic fields in dense cores/clumps

Hsi-Wei Yen, Patrick M. Koch, Charles L. H. Hull, Derek Ward-Thompson, Pierre Bastien, Tetsuo Hasegawa, Woojin Kwon, Shih-Ping Lai, Keping Qiu, Tao-Chung Ching, Eun Jung Chung, Simon Coude, James Di Francesco, Pham Ngoc Diep, Yasuo Doi, Chakali Eswaraiah, Sam Falle, Gary Fuller, Ray S. Furuya, Ilseung Han, Jennifer Hatchell, Martin Houde, Shu-ichiro Inutsuka, Doug Johnstone, Ji-hyun Kang, Miju Kang, Kee-Tae Kim, Florian Kirchschlager, Jungmi Kwon, Chang Won Lee, Chin-Fei Lee, Hong-Li Liu, Tie Liu, A-Ran Lyo, Nagayoshi Ohashi, Takashi Onaka, Kate Pattle, Sarah Sadavoy, Hiro Saito, Hiroko Shinnaga, Archana Soam, Mehrnoosh Tahani, Motohide Tamura, Ya-Wen Tang, Xindi Tang, Chuan-Peng Zhang We compare the directions of molecular outflows of 62 low-mass Class 0 and I protostars in nearby ($<$450 pc) star-forming regions with the mean orientations of the magnetic fields on 0.05-0.5 pc scales in the dense cores/clumps where they are embedded. The magnetic field orientations were measured using the JCMT POL-2 data taken by the BISTRO-1 survey and from the archive. The outflow directions were observed with interferometers in the literature. The observed distribution of the angles between the outflows and the magnetic fields peaks between 15 and 35 degrees. After considering projection effects, our results could suggest that the outflows tend to be misaligned with the magnetic fields by 50+/-15 degrees in three-dimensional space and are less likely (but not ruled out) randomly oriented with respect to the magnetic fields. There is no correlation between the misalignment and the bolometric temperatures in our sample. In several sources, the small-scale (1000-3000 au) magnetic fields is more misaligned with the outflows than their large-scale magnetic fields, suggesting that the small-scale magnetic field has been twisted by the dynamics. In comparison with turbulent MHD simulations of core formation, our observational results are more consistent with models in which the energy densities in the magnetic field and the turbulence of the gas are comparable. Our results also suggest that the misalignment alone cannot sufficiently reduce the efficiency of magnetic braking to enable formation of the observed number of large Keplerian disks with sizes larger than 30-50 au.

32. Kinematical signs of dust trapping and feedback in a local pressure bump in the protoplanetary disk around HD 142527 revealed with ALMA

Hsi-Wei Yen, Pin-Gao Gu We analyzed the archival data of the continuum emission at six wavelengths from 3 to 0.4 mm and 13CO and C18O (1-0, 2-1, and 3-2) lines in the protoplanetary disk around HD 142527 obtained with the Atacama Large Millimeter/submillimeter Array. We performed fitting to the spectral energy distributions obtained at the six wavelengths with the gray-body slab models to estimate the distributions of the dust surface density and spectral index of dust absorption coefficient beta. We also estimated the distribution of the gas column density by fitting the C18O spectra and measured the disk rotation by fitting the Keplerian disk models to the C18O data. We found super- and sub-Keplerian rotation inside and outside the dust ring in the northwest in the HD 142527 disk, suggestive of the presence of a local pressure bump. In comparison with our estimated dust and gas distributions, the location of the pressure bump is coincident with the region showing a three times higher dust density and a three times lower gas-to-dust mass ratio than the mean values in the disk, suggesting dust trapping in the pressure bump. Nevertheless, there is no correlation between our derived beta distribution and the location of the pressure bump. In addition, we found that the width of the dust ring is comparable or larger than the width of the pressure bump, which could suggest that dust feedback is significant in the pressure bump.

33. Multi-epoch SMA observations of the L1448C(N) protostellar SiO jet

Tomohiro Yoshida, Tien-Hao Hsieh, Naomi Hirano, Yusuke Aso L1448C(N) is a young protostar in Perseus, driving an outflow and an extremely high-velocity (EHV) molecular jet. We present multi-epoch observations of SiO $J = 8 - 7$, CO $J = 3 - 2$ lines, and 345 GHz dust continuum toward L1448C(N) in 2006, 2010, and 2017 with the Submillimeter Array. The knots traced by the SiO line show the averaged proper motion is $\sim 0''.06$ yr^{-1} and $\sim 0''.04$ yr^{-1} for the blue- and red-shifted jet, respectively. The corresponding transverse velocities are ~ 78 kms^{-1} (blueshifted) and ~ 52 kms^{-1} (redshifted). Together with the radial velocity, we found the inclination angle of the jets from the plane of the sky to be ~ 34 deg for the blueshifted jet and ~ 46 deg for the redfshifted jet. Given the new inclination angles, the mass-loss rate and mechanical power were refined to be $\sim 1.8 \times 10^{-6}$ $M_\odot$ and ~ 1.3 $L_\odot$, respectively. In the epoch of 2017, a new knot is detected at the base of the redshifted jet. We found that the mass-loss rate of the new knot is three times higher than the averaged mass-loss rate of the redshifted jet. Besides, continuum flux has enhanced by $\sim 37\%$ between 2010 and 2017. These imply that the variation of the mass-accretion rate by a factor of ~ 3 has occurred in a short timescale of $\sim 10 - 20$ yr. In addition, a knot in the downstream of the redshifted jet is found to be dimming over the three epochs.

34. An X-ray View of Two Infrared Dark Clouds G034.43+00.24 and G035.39-00.33

Hanbo Yu, Junfeng Wang, Jonathan C. Tan We present a high spatial resolution Chandra X-ray study of two Infrared Dark Clouds (IRDCs), G034.43+00.24 and G035.39-00.33, which are expected to be in the early phases of star cluster formation. We detect 112 and 209 valid X-ray point sources towards G034.43+00.24 and G035.39-00.33, respectively. We cross-match the X-ray point sources with 2MASS, GLIMPSE and WISE catalogs and find 53have corresponding infrared counterparts, respectively. These sources are probable members of young massive clusters in formation, and using stellar isochrones we estimate that a population of 1–2 Myr old, intermediate to high mass young stellar objects (YSOs) exist in both IRDCs. Two and ten Class II counterparts to X-ray sources were identified in G034.43+00.24 and in G035.39-00.33, respectively, which are located in or near dark filaments. The X-ray Luminosity Function (XLF) of G035.39-00.33 implies that the total mass consists of up to $\sim 1,700\,M_\odot$ of stars, using the XLF of the well-studied Orion Nebula Cluster as calibrator. This corresponds to a star formation efficiency of at most 5gas dominated and in an early stage of the star formation process. The population of G034.43+00.24 is less well determined due to the lower sensitivity of its observations.

35. Confirming the Explosive Outflow in G5.89 with ALMA

Luis A. Zapata, Paul T. P. Ho, Manuel Fernández-López, Estrella Guzmán Ccolque, Luis F. Rodriguez, José Reyes-Valdés, John Bally, Aina Palau, Masao Saito, Patricio Sanhueza, P. R. Rivera-Ortiz, A. Rodriguez-González The explosive molecular outflow detected decades ago in the Orion BN/KL region of massive star formation was considered to be a bizarre event. This belief was strengthened by the non detection of similar cases over the years with the only exception of the marginal case of DR21. Here, we confim a similar explosive outflow associated with the UCH$_{\rm II}$ region G5.89$-$0.39 that indicates that this phenomenon is not unique to Orion or DR21. Sensitive and high angular resolution ($\sim 0.1''$) ALMA CO(2$-$1) and SiO(5$-$4) observations show that the molecular outflow in the massive star forming region G5.89$-$0.39 is indeed an explosive outflow with an age of about 1000 yrs and a liberated kinetic energy of 10^{46-49} erg. Our new CO(2$-$1) ALMA observations revealed over 30 molecular filaments, with Hubble-like expansion motions, pointing to the center of UCH$_{\rm II}$ region. In addition, the SiO(5$-$4) observations reveal warmer and strong shocks very close to the origin of the explosion, confirming the true nature of the flow. A simple estimation for the occurrence of these explosive events during the formation of the massive stars indicates an event rate of once every $\sim$100 yrs, which is close to the supernovae rate.